

The W boson mass: precision measurement and impact on physics

Ashutosh V. Kotwal
Duke University

September 13, 2024

Abstract

As a mediator of the weak nuclear force, the W boson influences many properties of fundamental particles and their interactions. Understanding the W boson as accurately as possible, including knowing its mass, has been a priority for decades. In a succession of measurements with increasing precision by multiple experiments, a significant tension between its measured and predicted mass has recently been documented by the CDF Collaboration. Smaller differences between measurements exist. As the W boson mass provides a window on new physics, a comparison between different measurement techniques can inform the path to further investigations.

1 Introduction

Ever since the discovery of the weak nuclear force in radioactive decays more than 100 years ago, this interaction has continued to be a source of intrigue and new insights into fundamental particles and their interactions at the smallest distances. Among other surprises, the weak nuclear force taught us that nature distinguishes between particles and their mirror images (so-called parity violation) (see [1] and references therein), and that fundamental particle masses are emergent properties arising from their interaction with the constant, non-zero value of the Higgs field in the vacuum [2, 3, 4, 5, 6, 7, 8].

The W boson, as one of the carriers of the weak nuclear force, plays a special role in the well-developed theory of fundamental particles referred to as the Standard Model (SM) [9, 10, 11]. Despite certain conceptual limitations [12], the SM continues to be extraordinarily successful in predicting the properties of fundamental particles and their interactions as witnessed by the spate of results obtained from experiments at the Large Hadron Collider (LHC) [13, 14].

However, the recent, high-precision measurement of the mass of the W boson [15] differs significantly (7σ) from its calculated value in the SM [16, 17, 18], becoming the latest surprise in fundamental physics that points towards inadequacies of the SM and opening

doors for further revelations. This measurement confirms the trend that almost all previous measurements have also been higher than the SM expectation (see Fig. 2); this measurement is the first to achieve the requisite precision to create a sharp inconsistency with the SM.

The direct observation of the W [19, 20] and Z [21, 22] bosons, the mediators of the weak interaction, at the CERN $Spp\bar{S}$ collider in 1983 was a major milestone in the understanding of fundamental particles and their interactions. Since then, the precise measurement of their masses has been one of the priorities of the subfield of particle physics that focuses on precision measurements. In a few years following their discovery, their masses were measured with a precision of 2-0.5% [23, 24, 25, 26, 27]. In the following two decades, the large electron-positron (LEP) collider at CERN [28, 29, 30, 31, 32, 33, 34, 35, 36] and the Tevatron proton-antiproton collider at Fermilab [37, 38, 39, 40, 41, 42, 43, 44, 45, 46] advanced these measurements. They surpassed 0.1% precision in the W boson mass [47] and achieved 23 parts per million precision in the mass of the Z boson [16]. With the precise measurements of the Z boson mass, the lifetime of the muon and the coupling strength of the electromagnetic interaction, as well as the masses of the top quark and the Higgs boson, the SM is able to calculate the expected mass of the W boson to an accuracy better than 0.01% [16].

Between 1995 and 2000, the Tevatron collider was upgraded to deliver a factor of 100 more data than its 1992-1995 run. This second run operated between 2000 and 2011. Along with many other physics goals, improving the precision of the W boson mass measurement to test the SM was a priority for the Tevatron experiments CDF and D0. Using the steadily increasing datasets, both CDF [48, 49, 50, 51] and D0 [52, 53, 54] produced multiple measurements of the W boson mass with increasing precision, reaching 0.02% in 2012 [55]. In parallel, the LHC started data-collection in 2009 and some of these data have been analyzed to publish M_W measurements by the ATLAS [56, 57] and LHCb [58] experiments, achieving precisions of 0.02% and 0.04% respectively. The latest result from CDF in 2022 uses the complete Tevatron dataset and achieves a precision of almost 0.01% [15]. This measurement reveals the 7σ tension with the SM expectation, prompting a flood of speculations on the implications for new physics.

The measurement of the W boson mass is substantially more complicated than the Z boson mass, even though both particles have clean two-body decay modes containing electrons or muons. Most of these complications arise from the presence of the neutrino in the W boson decay, which is undetectable while carrying away half of the rest-mass energy of the boson. The inference of the latter from the partial information available in the final state is one of the reasons that each iteration of the data analysis has required many years¹.

This article, which is part review and part perspective, recaps the role of m_W in the SM and its extensions, compares and contrasts m_W measurement techniques, and discusses prospects and future directions.

¹ W bosons also decay to quark-antiquark pairs. This mode has never been used to make a precise measurement of M_W at a hadron collider, because this mode is swamped by non- W background processes and because the measurement of the net 4-momentum of the daughter particles is not sufficiently precise or accurate.

2 Theoretical motivation

The mass of the W boson is a very interesting observable because there is a strong theoretical connection between the masses of the W and Z bosons in the SM, a relativistic quantum field theory of matter and its electromagnetic, weak and strong interactions. To understand this connection, we can imagine an inaccurate but simplest version of the weak interaction based purely on the $SU(2)$ gauge group. In the SM, the principle of gauge symmetry of the fermionic wave functions is invoked, under which the fermions undergo transformations in an internal space while maintaining the invariance of the theory. The transformation is referred to as a gauge transformation when it is a smooth (but otherwise arbitrary) function of spacetime. The manifold of these symmetry transformations is described by a chosen Lie group, which is referred to as the gauge group.

The simplest gauge group is $U(1)$ whose manifold is a circle; therefore this gauge transformation changes the phase of the wave function smoothly with respect to spacetime. The principle of gauge symmetry states that the fermion's equation of motion should be invariant under these arbitrary transformations. This is accomplished by corresponding changes in the induced vector potential by the spacetime derivative of the arbitrary phase function. The theory with this choice of gauge group describes fermions with electromagnetic interactions. The generators of the Lie group are identified with the vector bosons that mediate the interaction; the $U(1)$ generator is identified with the photon.

When the gauge group is $SU(2)$ (whose manifold is the unit 3-sphere S^3), the fermions are described in the internal space by two components that transform into each other under the action of the symmetry. As a gauge transformation, it is again local, i.e. it is a matrix-valued function of spacetime. Therefore, the induced vector potential is also matrix-valued, and couples the two components of the fermion wave function to each other. For the weak interaction, the vector bosons thus mediate transformations between the electron and the electron-neutrino, between the up and down quarks and in general between the two components of the weak- $SU(2)$ doublet of fermions.

Infinitesimal $SU(2)$ group transformations have a correspondence with infinitesimal rotations of a sphere. The basis vectors of a two-component fermionic wave function may be visualized as the poles of the sphere². This is in analogy with $SU(2)$ being used to describe rotations of electrons in space, where the components of the spinors of $SU(2)$ describe the spin-up and spin-down states of electrons. Continuing this analogy, the weak interaction transforms a fermion doublet from one component to the other by the emission or absorption of a W boson. This description requires the existence of a third transformation that can be visualized as a rotation along the equator of the sphere. Thus, the $SU(2)$ gauge group predicts three gauge bosons, which mathematically serve as the generators of group transformations and physically mediate all possible weak interactions. In this simplest picture, the three types of interactions associated with the weak force must be exactly symmetric because they are related by the rotational symmetry.

²This analogy captures some of the properties of the $SU(2)$ action, but not all of them. Precise mathematical discussions can be found elsewhere.

The principle of symmetry under gauge transformations (called gauge invariance) predicts that these transformations must be induced by massless gauge bosons in the relativistic quantum theory. This principle has served to beautifully explain the massless photon as the gauge mediator of the electromagnetic interaction, and the massless gluons as the mediators of the strong nuclear force when probed at high energies.

The weak interaction, on the contrary, appears to be mediated by very massive bosons, which explains why this interaction appears to be “weak” at low energies. This mystery led to the postulate of the Anderson-Brout-Englert-Higgs-Guralnik-Hagan-Kibble mechanism [2, 3, 4, 6] in which the Lorentz-invariant Higgs field develops a constant, non-zero value in the vacuum. The interactions of all particles experiencing the weak force with this Higgs condensate imparts the emergent property of mass to them as a low-energy manifestation.

In this simplest description of the weak-interaction group, the three gauge bosons will acquire the same mass because of their mutual rotational symmetry - the two W bosons and the third would-be Z boson. From this starting point, we can sequentially incorporate the known principles of nature that modify the original rotational symmetry. The biggest effect is the quantum-mechanical mixing between the third $SU(2)$ generator and another, electromagnetism-like $U(1)$ interaction called hypercharge, yielding the observed Z boson and the photon (γ) as the mixed states [9]. The Higgs field is an $SU(2)$ doublet. The quantum numbers of its condensate are such that one of the mixed states remains massless; this state is identified as the photon [10, 11]. In other words, while the condensate (i.e. the true vacuum) is charged under $SU(2)_{\text{weak}}$ and under $U(1)_{\text{hypercharge}}$, the linear combination of these charges that is identified as electric charge is zero for the condensate. Therefore the vacuum is electrically neutral, gauge invariance is maintained for electromagnetism, electric current is conserved and the photon is massless. However, the weak charge and hypercharge of the Higgs condensate ensure that the W and Z bosons acquire masses whose values are proportional to their respective dimensionless coupling to the condensate and the energy-dimensioned value of the latter. This means that the weak current and the hypercharge current are not separately conserved after the Higgs condensate forms [10, 11].

The electromagnetic fine structure coupling α , the Fermi coupling constant G_F (extracted from lifetime of the muon) and the Z boson mass are the most precisely measured observables [16] related to the three parameters of the theory; the $SU(2)$ and $U(1)$ gauge couplings and the value of the Higgs condensate. With the tight constraints on the parameters from these measurements, the theory is rendered predictive for M_W . In other words, the theory predicts M_W when α , G_F and M_Z are fixed to their measured values [59],

$$M_W^2 \left(1 - \frac{M_W^2}{M_Z^2}\right) = \frac{\pi\alpha}{\sqrt{2}G_F} (1 + \Delta r)$$

where Δr denotes the quantum-mechanical radiative corrections (explained in the next paragraph) and classical physics predicts $\Delta r = 0$. The mixing between one of the $SU(2)$ generators and the $U(1)$ generator violates the original rotational symmetry (called custodial symmetry) between the three $SU(2)$ generators; the Z boson mass differs from the W boson mass, with $M_Z > M_W$ since $M_\gamma = 0$. M_W is thus a probe of such custodial symmetry-

violating effects, which makes its precise measurement of high importance to check for a deviation from the calculated value [60].

The $SU(2)\times U(1)$ mixing effect is within the realm of classical physics. In the 1990's, the precision of the M_W measurement became sufficient to discern the small quantum effects denoted by Δr ; these are due to vacuum fluctuations wherein particle-antiparticle pairs appear and disappear over very short time intervals, consistent with the Heisenberg uncertainty principle and special relativity. The gauge bosons experience quantum fluctuations into fermion-antifermion pairs [61].

From the perspective of the W boson mass, the most interesting fluctuations involve the top quark and the bottom quark, members of a weak- $SU(2)$ doublet. However, their interaction with the Higgs field is very different, resulting in a large difference in their masses and also a large violation of the custodial symmetry that tries to maintain the similarity of the W and Z boson masses. Hence, quantum fluctuations in the gauge boson propagators involving weak- $SU(2)$ doublet components with different masses induce a calculable modification of M_W for a fixed M_Z ; this modification is dominated by fluctuations into top-bottom quarks which have by far the largest mass difference among all $SU(2)$ doublets. In other words, mass differences between weak- $SU(2)$ doublet fermions represent another violation of the custodial symmetry and therefore induce a shift in M_W through quantum effects [62].

Historically, an estimate of the top quark mass was inferred from such quantum corrections [63]. Since the top quark discovery by the CDF [64] and DØ [65] experiments at the Tevatron in 1995, its mass has been measured directly and included as an input in the calculation [16]. Finally, quantum corrections involving the Higgs boson also induce a shift in the expected value of M_W [66], and this became a method for inferring the Higgs boson mass before the latter was directly observed.

This history illustrates how the W boson mass, in conjunction with other measurements, has been a harbinger of fundamental principles of nature. Looking to the future: with increasing precision, M_W can probe additional laws of physics that may follow this pattern of custodial-symmetry violation between the W and Z bosons. Hypotheses include a new, weak force (which might mediate an interaction with dark matter) that mixes with the photon and the Z boson, the existence of additional Higgs-like bosons that interact differently with W versus Z bosons, and heavy, weakly-interacting fermion or boson pairs that have a large mass difference akin to the top-bottom mass difference.

A popular hypothesis that accommodates the latter is supersymmetry, in which all SM particles have supersymmetric partners whose intrinsic spin differs by $\hbar/2$ from their respective SM counterparts³. Such heavy particles may also arise as composite states due to substructure and a new strongly confining interaction at the TeV energy scale. This new interaction and substructure may provide a dynamical explanation for the formation of the Higgs condensate, and the Higgs boson may be a bound state rather than the fundamental scalar of the SM. Conceivably, this new dynamical sector is connected with dark matter particles, or with the mystery of the excess of matter over antimatter in the universe, or both. Both supersymmetry and compositeness allow for a new conserved quantum number

³The reduced Planck's constant $\hbar \equiv h/(2\pi)$ is the fundamental unit of angular momentum.

that stabilizes one or more of the new particles which, if interacting very weakly with SM particles, can constitute the dark matter.

These are some of the hypotheses being investigated as explanations of the difference between the CDF measurement and the SM expectation of M_W .

3 Measurement of the W boson mass

The W boson mass has been measured both at proton-(anti)proton colliders and electron-positron colliders. It is healthy for the scientific development of the field to perform measurements under different experimental circumstances and with different techniques.

The largest samples of W and Z bosons are produced at proton-(anti)proton colliders. The bosons are mostly produced singly from the annihilation of a quark and an antiquark respectively from the colliding beam particles (see Fig. 1). These initial-state particles are strongly-interacting, i.e. the principle of gauge symmetry with the gauge group $SU(3)$ explains the “strong” interactions between quarks as being mediated by gluons. Analogous to the electric charge associated with particles that interact electromagnetically, the “charge” quantum number associated with the strong interaction is called color. When a colored quark and antiquark collide to produce a colorless electroweak boson, they are decelerated which causes them to radiate gluons. Thus, electroweak gauge boson production is accompanied by multiple radiated gluons which further split into quark-antiquark pairs. This shower of colored particles coalesces into a spray of color-neutral bound states called hadrons due to the color-confining nature of the strong interaction.

The decay products of the W boson provide insufficient information to fully reconstruct the quark-antiquark collision, due to the invisible momentum carried away by the neutrino. The measurement of the net momentum carried by the accompanying spray of hadrons is therefore necessary to recover as much of the missing information as possible.

The $SU(3)$ -gauge theory of strong interactions called quantum chromodynamics (QCD) has made enormous progress over the last five decades. In one of its great insights, the combined effect of quantum fluctuations involving quarks and gluons is to reduce the effective color charge as the energy of the scattering process increases [67, 68]. This property of asymptotic freedom of QCD makes it possible to calculate high-energy QCD-radiative processes in perturbation theory. However, perturbation theory becomes progressively inaccurate when the relevant process energy decreases to the GeV level and the effective QCD coupling is no longer small enough.

3.1 Sensitivity to QCD calculations

The inference of the neutrino momentum is aided by the use of theoretical calculations of W boson production and decay, that take into account the effects of the strongly-interacting QCD radiation. Over the decades, these calculations have progressed in accuracy by including quantum-mechanical amplitudes at higher order in perturbation theory.

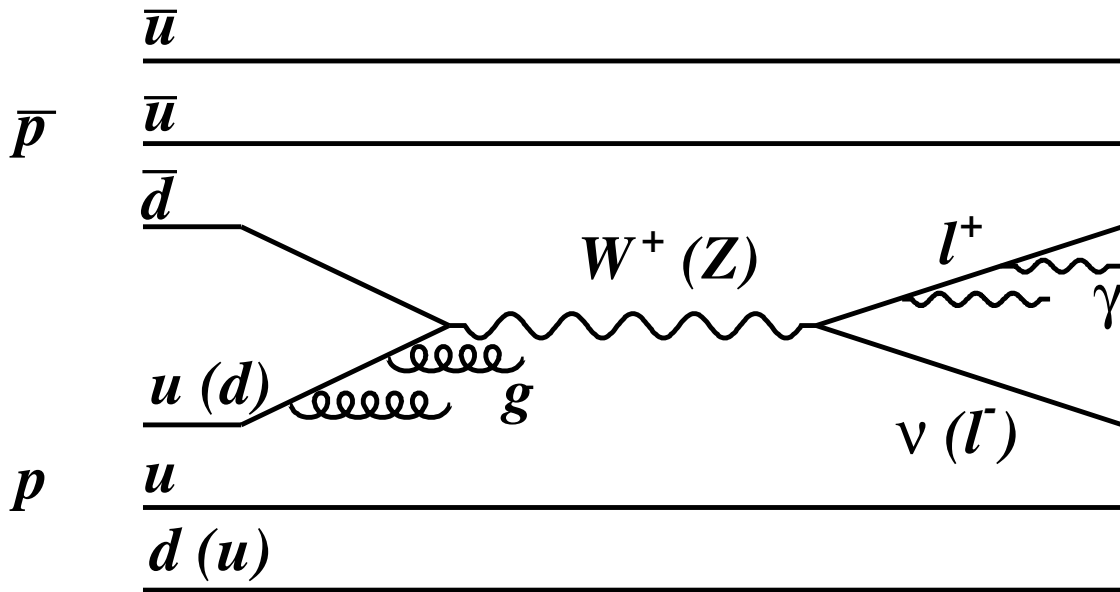


Figure 1: Illustration (reproduced with permission from Ref. [51]) of W (or Z) boson production due to quark (q) – antiquark (\bar{q}) annihilation in $p\bar{p}$ collisions at the Tevatron, where the initial-state q (\bar{q}) are predominantly intrinsic to the proton p (antiproton \bar{p}). Quarks associated with the annihilation to a Z boson are indicated in parentheses. Initial-state gluon (g) radiation and final-state photon (γ) radiation are also shown. The initial state QCD radiation fragments into a spray of hadrons. At the LHC, the initiating \bar{q} arises from $g \rightarrow q\bar{q}$ splitting.

An important theme in the M_W measurement is the ability to improve the accuracy of these calculations by applying constraints from the data. In this respect, the Tevatron has some advantages over the Large Hadron Collider (LHC). At the Tevatron, antiprotons already contain antiquarks, whereas the latter have to be generated through the strong interaction radiative processes when using proton beams at the LHC [56, 57]. Second, the fractional momenta of the (anti)quarks with respect to the (anti)protons at the Tevatron are larger, and their probability distributions are better measured and less affected by QCD radiation, in comparison to the corresponding distributions at the LHC [15]. Third, W boson production at the Tevatron is minimally induced by the heavy bottom, charm and strange quarks, which do contribute significantly at the LHC [56, 57] and whose effects are difficult to calculate.

Within the general theme of constraining the QCD modeling of W boson production with measurements of the accompanying QCD radiation, there are differences between the methodologies used by the Tevatron experiments (CDF and D0) and the LHC experiments (ATLAS and LHCb, with the first measurement from the CMS experiment to be expected).

The Tevatron experiments have consistently used a calculation of vector boson production that includes the effects of multiple soft-gluon radiation and gluon splitting into quark-antiquark pairs, coupled to an exact calculation of a single energetic gluon emission or gluon splitting [69, 70, 71]. There has been discussion of this boson production and decay calculation in the context of the recent, highest-precision measurement of the W boson mass by the CDF experiment [15, 72]. One of the discussion points is the effect of double gluon radiation or gluon splitting with high transverse momentum (p_T). Three facts shed light on this point.

First, the phase space of the W bosons selected for this analysis is confined to small p_T , where the “resummation” of multiple gluon emission and splitting is the most relevant description of the boson production process. The so-called “fixed-order” calculation of individual emissions is already a minor correction in this phase space. Second, the calculation is tuned on the observed p_T spectrum of the Z boson, which constrains the QCD parameters that are largely identical between Z and W boson production. All hadron collider experiments follow this strategy.

Third, a unique feature of the CDF measurement is the direct application of the W boson p_T data as an additional constraint on the corresponding calculation. The perturbative QCD calculation of the W boson p_T spectrum may not be sufficiently accurate even after the calculation has been adjusted so that the calculated and the measured Z boson p_T spectra agree. The residual variation in the calculated p_T^W spectrum due to unconstrained degrees of freedom has an impact on the M_W measurement. However, no other experimental analysis has constrained the calculation of the W boson p_T spectrum with the corresponding observed distribution in the signal sample, as CDF has.

This constraint would be difficult to apply for the LHC experiments because of the degraded resolution on p_T^W due to the large number of additional beam-beam interactions occurring simultaneously (called pile-up events) at the LHC. Tevatron experiments have the advantage of running with lower pile-up, which permits CDF to measure p_T^W with adequate

resolution to apply this constraint.

In this context, the details of W versus Z boson production merit a discussion. For massless initial-state quarks (a valid approximation at the Tevatron), CDF has used the DYqT calculation [73, 74] to confirm that the p_T^W and p_T^Z spectra would be identical if the bosons had the same mass. Therefore, the difference between W and Z bosons in the flavor composition of the initial-state quarks does not impact perturbative-QCD processes. The difference in the boson mass scales, however, does change the phase space available for QCD radiation and impacts the p_T^W/p_T^Z ratio of spectra. The variation in this ratio can be parameterized in terms of the renormalization, factorization and resummation scales (in increasing order of sensitivity) which capture the perturbative inaccuracy of the QCD calculation. CDF constrained this parameterization using the measured W boson p_T spectrum. In the context of perturbative QCD, the concern that the tuned Z boson production model may not be portable to W bosons has been addressed directly only by the CDF analysis.

In the ATLAS analysis [56, 57] an attempt is made to check the theoretical p_T^W/p_T^Z spectrum ratio against a low-precision measurement made with $\mathcal{O}(1\%)$ of the M_W -measurement dataset. Calculations are also compared with the tail of the observed distribution of the component of \vec{p}_T^W along the charged-lepton direction. This quantity is presented as a kind of proxy for p_T^W and used to reject certain calculations of the p_T^W/p_T^Z spectrum ratio.

In the LHCb analysis [58], a measurement of \vec{p}_T^W is not possible because the detector does not surround the beam collision point. An attempt is made to gain sensitivity to the p_T^W spectrum by floating an additional nuisance parameter in the fit to the q^μ/p_T^μ spectrum of muons (of charge q^μ) from $W^\pm \rightarrow \mu^\pm \nu$ data. This parameter converges to a different value from the one that best fits the p_T^Z data. If they are constrained to a common value, the inferred M_W increases by 39 MeV, though the quality of the fit degrades. This situation illustrates why a direct constraint from p_T^W data, as obtained by CDF, is preferable to the use of a proxy or multivariate fits with hidden dependencies that are difficult to control.

At very low boson p_T , the effective strong-interaction coupling becomes large enough that non-perturbative QCD processes dominate, which may differentiate between Z and W bosons. In the limit of massless quarks, this possibility is considered in the CDF analysis by including a mass-dependence in the non-perturbative parameters. One parameter is constrained with the CDF data on the Z boson, and a published global fit is used for the second parameter. The global fit includes the measured p_T spectra of low-mass vector bosons [71]. As this global fit was performed about 20 years ago, it would be useful to repeat it with new data on low-mass boson production and with newer calculational tools, to help confirm the robustness of the CDF analysis in this respect.

In summary, all hadron collider analyses of M_W tune parameters of the QCD calculation of boson production to match the observed p_T^Z distribution. Other than CDF, all other analyses assume that the tuned calculation automatically describes W boson production accurately, though additional parameters are known to differentiate between W and Z boson production. What sets the CDF analysis apart is its use of the observed p_T^W distribution to constrain the most important of these parameters, demonstrating its reliability in this respect.

3.1.1 Theoretical issues in non-perturbative QCD

The preceding discussion of electroweak boson production, framed in the context of massless quarks, suggests the following investigation. A fraction of W bosons are produced with a charm quark in the initial state, whose mass of ≈ 1.3 GeV may induce a non-perturbative effect that differentiates W from Z boson production and spoil the portability of the Z boson production model to W bosons. At the Tevatron, only a small percentage of W boson production is induced by charm quarks, while this fraction is many times larger at the LHC. The effect of the charm quark mass is expected to be negligible at the Tevatron; a definitive confirmation requires a QCD calculation that includes the charm quark mass. Such a calculation would be a welcome addition in the domain of high-accuracy QCD calculations of electroweak boson production. Similar considerations apply for bottom quark-induced Z boson production at the LHC. Since heavy-quark mass effects are a source of systematic uncertainty at the LHC, M_W measurements at the LHC would benefit.

Another aspect of non-perturbative QCD is worth exploring. The wave functions of up and down quarks in nucleons are governed by non-perturbative QCD dynamics. Since there is a net of two up quarks and one down quark in the proton, Fermi-Dirac statistics suggests a difference between the up- and down-quark wave functions and their intrinsic p_T . As the mix of up and down quarks differs between W and Z bosons, the intrinsic p_T difference may lead to small differences in the W and Z boson p_T spectra at small p_T [75]. This is another example of non-perturbative effects that can spoil the portability of the p_T^Z spectrum parameters to the p_T^W spectrum. The quark-flavor dependence of the intrinsic p_T is not known; its theoretical investigation would benefit all hadron-collider analyses of M_W .

Thus, improvements in the theoretical understanding of heavy quarks and of the flavor-dependent non-perturbative aspects of proton structure would help to port the Z boson model to W bosons at very low p_T .

3.2 Momentum calibration of the experiment

One of the most important aspects of the M_W analysis is the calibration of the momentum of the charged lepton (electron and muon) emitted in the W boson decay. Charged-particle momenta are measured using a magnetic tracker, consisting of position-measuring sensors arranged in a concentric cylindrical configuration and immersed in an axial magnetic field. The position measurements along the helical trajectories are used to infer the curvature, the direction, and in conjunction with the magnetic field, the momentum vector. Electrons and photons are measured using electromagnetic calorimeters that convert the particle's energy into a shower of soft photons and electron-positron pairs in the nuclear electric field of a dense material. As this cloud of charge traverses instrumented active material, it creates scintillation light or ionization which is converted to a proportional electrical signal as a measure of the incident electron/photon energy.

The momentum calibration philosophies followed by the hadron-collider experiments fall into two categories, one followed by the ATLAS, DØ and LHCb experiments and the other followed by the CDF experiment.

The ATLAS and DØ experiments make no attempt to calibrate the magnetic tracker from first principles. Instead, they calibrate solely on the Z boson mass, i.e. adjust the detector response functions until the Z boson mass measured using the adjusted lepton momenta agrees with the previously measured precise value from the LEP collider. At first glance this procedure seems sound since $M_Z = 91.19$ GeV is similar to $M_W \approx 80.4$ GeV and the calibration has to be ported over a fraction of the relevant momentum range.

However, the difference between M_W and M_Z is 11 GeV; when the M_W measurement reaches the precision level of 10^{-4} there is no *a-priori* proof that porting the M_Z -based calibration to M_W is fundamentally understood at the 10^{-3} level. In more than three decades of M_W measurements at hadron colliders, the sole reliance on M_Z for calibration has never been formally proven to be sufficiently accurate.

The M_W analysis from the complete Tevatron Run 2 dataset by the DØ experiment is an instance where the M_Z -based calibration strategy did not ultimately succeed. The DØ experiment has not analyzed the latter 40% of Run 2 data, apparently due to tracker degradation [76]. The larger implication is that calibration on M_Z alone is insufficient for the requisite accuracy and robustness, due to a dependence on tracker information. This operational experience and its relevance for M_W measurement would be useful to document.

Cognizant of potential weaknesses of a solely M_Z -based calibration, all three CDF publications from Run 2 data emphasized a more robust calibration and analysis strategy from the beginning. In contrast with the other analyses, the CDF procedure for charged-lepton momentum calibration relies on fundamental principles of operation of the sensor technologies. The first step is the alignment and calibration of the drift chamber [77], which yields the calibrated track momentum of all charged particles. CDF has developed a special technique using cosmic rays [78] to pin down the positions of the 30,240 sense wires in the drift chamber to a precision of ≈ 1 μm , eliminating many biases in the measurement of track parameters [79]. The procedure was refined over three iterations in the last two decades, each iteration requiring between one and two years.

Cosmic rays provide the most direct and transparent method of aligning the position-measuring sensors. As these muons rain down on the detectors from the atmosphere, they traverse the tracking sensors diametrically across their cylindrical geometry. This trajectory builds in a powerful redundancy because the same muon is measured twice, on opposite sides of the beam axis. In the CDF procedure, a single helical fit is performed to this double-sided trajectory [78]. This fit is immune to many of the deformations of the tracker that bias collider tracks; the latter are prone to bias because they propagate outwards from the beam axis. Due to this intrinsic rigidity, the double-sided fitted trajectory of the cosmic ray provides the most robust reference with respect to which the sensors can be aligned, thus eliminating the deformation-induced bias [79]. Given the large size of the cosmic-ray sample at CDF, different sensors overlap sufficiently that they are all anchored with respect to each other with a precision of ≈ 1 μm .

The CDF procedure emphasizes the importance of control; the observable(s) chosen for calibrating any parameter(s) should (i) be a strong function of the parameter(s) of interest, and (ii) be as independent as possible of other variables. The latter is a crucial consideration

because it minimizes the chance of being misled in the parameter inference. Both requirements are strongly satisfied by the CDF cosmic-ray alignment procedure – it isolates the degrees of freedom of the sensor positions and is almost independent of other variables. It is then possible for CDF to analytically identify the remaining modes of displacement that cannot be measured by the cosmic-ray method; these are pinned down using complementary techniques [15]. These features distinguish the CDF tracker alignment from the procedure published by, for example, the LHCb experiment [58].

The next step in the CDF procedure is the calibration of the magnetic field and its spatial non-uniformity using the reconstructed invariant mass of the J/ψ particle, whose mass is precisely known, in its dimuonic decay channel. This large sample enables a fine-grained spatial scan of the drift chamber. These muons also cover a wide range in track curvature, the quantity directly measured by the drift chamber, and enable the calibration of momentum-dependent effects such as the ionization energy loss in the passive material [15, 49, 51].

Additionally, CDF uses a large sample of Υ particles decaying to dimuons to demonstrate the consistency and robustness of the tracker calibration. First, Υ s with a higher (and again precisely known) mass than the J/ψ cover the phase space closer to W bosons. Second, the muon tracks used for the $\Upsilon \rightarrow \mu^+\mu^-$ mass calculation can be reconstructed with two variants of the track reconstruction algorithm. The consistency of the measured Υ mass between these variants is another important demonstration of the robustness of the momentum calibration [15, 49, 51].

Instead of a purely empirical calibration of the electromagnetic calorimeter, CDF performs a detailed first-principles simulation of electron and photon detection [80] based on the knowledge of the calorimeter geometry and electromagnetic showering calculations encoded in the GEANT program [81, 82]. Next, CDF uses the electrons emanating from W boson decay, with their calibrated momenta from the tracker, as an *in-situ* test-beam to measure the calorimeter thickness, non-linear energy response due to scintillator ageing, spatial and temporal variations in response, and the amount of passive radiative material upstream of the tracker. Almost all tuned parameters are causally related to the principles governing electron and photon interactions with various materials [15, 49, 51].

The ultimate confirmation of these calibration procedures is the independent measurement of the Z boson mass by CDF in both electron and muon channels, using the same “blinded” procedure as used for the M_W measurement, and demonstrating consistency with the LEP value. Amongst all hadron-collider measurements of the W boson mass, the three CDF measurements published from the Tevatron Run 2 data are unique in pursuing these high-precision calibrations and cross-checks from first principles [15, 49, 51]. All other hadron collider measurements have been based solely on rescaling various observables based on the reconstructed Z boson mass.

The LHCb experiment uses a mix of $J/\psi \rightarrow \mu^+\mu^-$, $\Upsilon \rightarrow \mu^+\mu^-$ and $Z \rightarrow \mu^+\mu^-$ data to understand the tracker. Misalignments are parameterized by corrections to the track curvature and the parameters are fitted using a proxy for the reconstructed Z boson mass in the data. The momentum scale and resolution parameters are fit simultaneously to the J/ψ , Υ and Z boson data; however the mutual consistency of the momentum calibration

from independent datasets is not demonstrated [58].

For the M_W measurement, the CDF strategy benefits from unique features of its drift chamber geometry and construction, features that are lacking in the trackers of the other hadron-collider experiments. The CDF drift chamber is a single gaseous volume with embedded sense wires. Groups of twelve wires (cells) are mounted on precision-installed cards at each end of the cylindrical chamber, substantially reducing the number of alignment degrees of freedom [77]. In comparison, the LHC experiments use silicon sensor-based trackers which consist of many tens of thousands of small modules, leading to an explosion in the alignment degrees of freedom and a corresponding increase in tracker complexity for fundamental understanding.

The second advantage conferred by the CDF drift chamber is that, as a charged particle traverses 96 sense wires radially, there are no gaps or discontinuities in the instrumented volume. All particles must pass through 96 drift regions in which their positions are recorded, without exception. In particular, for incremental changes in the particle's curvature or direction, the relevant active regions change continuously and smoothly, with a handful of transitions between adjacent drift cells. This is the reason the curvature response function for this drift chamber is analytic, i.e. the measured track curvature is a smooth function of the true curvature and can be expressed as a polynomial function. Pinning down the few relevant polynomial coefficients is at the heart of the CDF tracker calibration.

In comparison, silicon trackers provide a factor of ten fewer (but substantially more precise) measurements, with many more boundaries between instrumented regions. It is more difficult to guarantee an analytic curvature response with few measurements along the track and a highly tiled detector geometry, which is inevitable when covering a large area with numerous small planar sensors.

To be sure, silicon trackers provide considerably higher performance than drift chambers in terms of precision, rate capability, granularity, radiation hardness and the ability to operate in high-flux environments. They are also uniquely suited to be placed close to the beam interaction point and measure the track impact parameters with high precision. It is the geometrical complexity and segmentation of silicon trackers that the curvature measurement is particularly sensitive to, because curvature is related to the second radial derivative of position whereas impact parameter is related to the first derivative. And for the m_W measurement, it is the track curvature that is crucial for the accurate inference of the transverse momentum, while the impact parameter is irrelevant because the daughter leptons are prompt.

This discussion motivates further studies of tracker geometries and an exploration of geometrical deformations that lead to a non-analytic curvature response at small curvature. It behooves the experiments to conduct such studies in order to fully understand and exploit magnetic trackers for precision measurements. It would be natural for CDF to lead these studies as they are most advanced in the systematic understanding of tracker-based momentum calibration.

In the spirit of making the most reliable measurement possible, it is crucial that the M_W analysis be based on fundamental principles which are transparent and are in the pub-

lic domain. CDF’s strategy for calibrating the charged-lepton momentum exemplifies this philosophy.

3.3 Event selection

The upside of W boson production at hadron colliders is that the production rate is substantially higher than at electron-positron colliders (e.g. LEP II); the complication is that this rate is less than one-millionth of the total hadron-hadron interaction rate. Real-time filtering to record events of interest while rejecting 99.99% of the uninteresting collisions is a crucial aspect of the experimental techniques at hadron colliders. In the offline analysis of the recorded data, further requirements are placed on the event information to suppress high-rate backgrounds from QCD-induced non- W events that mimic high- p_T electrons/muons along with a p_T imbalance due to resolution, faking a neutrino signature.

It is important to minimize the selection bias on W -boson events while also minimizing the misidentification backgrounds. Both effects alter the shape of the kinematic distributions from which M_W is inferred. The larger the bias, the more accurately it must be estimated from control samples of data or high-quality simulation.

Of the hadron collider experiments, CDF has the highest charged-lepton trigger efficiency and the smallest misidentification backgrounds; for W boson events selected with the charged-lepton $p_T^\ell > 30$ GeV for the analysis, the trigger efficiency is essentially 100% with no dependence on p_T^ℓ . As shown in Fig. S40 of [15], the inferred M_W is stable with respect to the p_T^ℓ requirement; no correction for trigger inefficiency is needed here. This is a substantial simplification compared to the p_T -dependent trigger inefficiencies in the ATLAS, DØ and LHCb experiments, which must be estimated and corrected for to prevent biasing the inferred M_W . The dependence of the selection bias on event topology is also the smallest in the CDF analysis, where the simplest selection requirements are sufficient to achieve charged-lepton misidentification backgrounds $< 0.4\%$.

The amount of QCD radiation accompanying the W bosons and the number of pile-up events are both much smaller at the Tevatron than at the LHC. Small pile-up implies that the resolution on the inferred p_T of the neutrino, p_T^ν is much better at the Tevatron. Both circumstances force the W boson selection to be $p_T^W < 30$ GeV in the ATLAS analysis, which is suboptimal compared to the $p_T^W < 15$ GeV requirement in the CDF and DØ analyses. The former admits more misidentification background, more QCD radiation, more corrections for efficiency-related biases, and considerable smearing of the kinematic distributions sensitive to M_W , all of which increase the experimental and theoretical complications associated with LHC measurements of M_W .

One concludes that the CDF experiment requires the smallest corrections for trigger- and selection-induced biases among the hadron collider experiments. This is an intrinsic advantage in CDF’s favor in terms of robustness of the analysis.

3.4 Hadronic recoil measurement

The \vec{p}_T^ν vector is inferred by measuring the \vec{p}_T vector of all detectable particles, and imposing \vec{p}_T -balance assuming a single neutrino in the event. In addition to the charged lepton(s) from $W(Z)$ boson decay, the initial-state QCD radiation which fragments into a spray of hadrons must also be measured (see Fig. 1). The vector sum \vec{u} of these hadrons' \vec{p}_T is referred to as the hadronic recoil vector, since it represents the measurement of $-\vec{p}_T^{W(Z)}$ using the hadrons. The response and resolution functions that characterize the \vec{u} measurement are more complicated than those for electrons and muons; fortunately the required accuracy is in parts per thousand rather than tens of parts per million for the charged leptons.

At a hadron collider, most of the beam particles' energy is transferred to collision fragments that propagate at small angles along the beam pipe and cannot be detected. Hence energy and momentum conservation cannot be used to infer the neutrino's longitudinal momentum; one can work with its \vec{p}_T vector only.

Three kinematic quantities are sensitive to M_W ; the distributions of p_T of the charged lepton and the neutrino, and the transverse mass m_T which is akin to the invariant mass but uses the leptons' \vec{p}_T vectors. The maximum value of the leptons' p_T (i.e. the distributions' approximate endpoint) is linear in M_W , but is also linear in boson p_T . The latter is incorporated from an accurate calculation, as discussed in Sec. 3.1, and measured as \vec{u} . Both inputs are important because neither is sufficient. The special property of the m_T distribution is that its endpoint does not depend on the boson's boost, while still being linear in M_W . This linear dependence on M_W is used to infer the latter from the shape of these distributions.

The M_W extraction from the p_T^ν distribution is by far the most sensitive to the imperfections of \vec{u} . Contrary to popular misconception, the use of the charged-lepton p_T^ℓ distribution is far from immune to the latter. The m_T -based extraction has yet another set of correlated dependencies on the various inputs. One of the strengths of the Tevatron analyses is that the benefits of the m_T variable are fully exploited, because the small pile-up maintains good resolution on \vec{u} . In fact, as shown in the CDF and DØ analyses, the \vec{u} -resolution is good enough to permit a reasonably precise extraction even from the p_T^ν distribution [15, 54].

The \vec{p}_T^ℓ vector plays the same role in all three kinematic distributions; they differ only in the usage of \vec{u} . Hence, the consistency of the M_W values inferred from these three distributions is the most powerful cross-check on the validity of the \vec{u} measurement and the associated uncertainties. The covariances of these M_W values with respect to the response and resolution functions of \vec{u} are used to quantify their mutual consistency. These consistency checks have been published by CDF [15, 49, 51]. An additional check to examine the consistency of M_W measurements in bins of pile-up would be useful for CDF to investigate.

Unfortunately, the \vec{u} resolution is quite degraded at the LHC due to the larger pile-up, to the extent that the m_T - and p_T^ν -based extractions are almost powerless in providing a validation of the \vec{u} measurement. Yet, the p_T^ℓ -based extraction, which is essentially the sole method of M_W inference at the LHC, is sensitive to a mismeasurement of \vec{u} through the event-selection criteria. As such, the LHC measurements of M_W lack the ability to demonstrate their robustness with respect to the hadronic recoil measurement in the same

way that CDF has demonstrated. The alternatives pursued in the ATLAS analysis are not as powerful [56, 57]. For example, the W -like reconstruction of the Z boson mass (Fig. 16 of [56]) is inconclusive at best.

This weakness can be rectified by analysis of the low pile-up data recorded at the LHC for the M_W measurement. In the CDF analysis, the $m_T:p_T^\ell:p_T^\nu$ -based extractions contribute in the proportion 64:26:10 in the combined final answer, while in the ATLAS analysis the p_T^ℓ -based extraction provides 95% of the final answer [83]. Even the p_T^ν -based extraction at CDF is more impactful than the m_T -based extraction at ATLAS. These weights illustrate the usefulness of the low pile-up data at the LHC.

On a related note, the component of \vec{u} parallel to the charged-lepton direction is important; it contributes linearly to the leptons' p_T . In the CDF analysis, special attention is devoted to the understanding of this component and its implications, as documented extensively in each of the three CDF publications from the Tevatron Run 2 data. A corresponding exposition in future ATLAS publications would be welcome, as there is currently little discussion of this key issue.

The point to emphasize is that the lower pile-up confers a significant advantage to the Tevatron over the LHC, which CDF has fully exploited to show cross-checks of the hadronic recoil measurement.

3.5 Likelihood fitting

Inference of parameters of interest (POI) from data is the domain of statistical analysis. The accurate description of the data is also controlled by many other “nuisance” parameters; so named because they need to be constrained in order to extract the POI, but are not the motivation for the analysis. When the POI is M_W , the nuisance parameters are related to the boson production and decay physics, the detector response and resolution functions and the non- W processes contaminating the data sample. The typical method of statistical inference is likelihood maximization, where the likelihood function depends on the POI(s) and the nuisance parameters.

There is a divergence on the choice whether to float the POI and the nuisance parameters separately or simultaneously. Two schools of thought have emerged. The traditional, conservative and time-tested methodology in precision measurements is to float them separately. The first step is to constrain all nuisance parameters from independent control samples of data, selected to be strongly constraining on the nuisance parameters while being independent of M_W . For each nuisance parameter, a causal and explainable logic is developed whose reasoning can be debated and improved, leading to scientific learning and progress. Likelihood maximization on these control data with respect to the nuisance parameters provide well-understood constraints on the latter. In the next step, the likelihood with respect to M_W is maximized on the m_T or the lepton p_T distributions of the data, while the nuisance parameters are fixed to their respective values determined from causal analysis of the control data. The covariance of M_W in the nuisance parameter space is estimated by varying the nuisance parameters by their *a-priori* justified uncertainties and noting the induced shift in

the fitted value of M_W . The covariance is determined from the model of the data so that it does not suffer from data-driven statistical fluctuations. This methodology, applied by the Tevatron experiments, has steadily advanced our fundamental understanding of the nuisance parameters and their impact on the M_W extraction, as documented in a set of detailed publications [27, 38, 39, 41, 43, 45, 46, 49, 51, 54, 15]. It is considered a robust, interpretable and transparent method of data analysis because it clearly demarcates between the POI and the nuisance parameters and maintains their meaning.

The newer school of thought approaches precision analysis as a machine learning exercise. The *a-priori* constraints on nuisance parameters from control data are sometimes weak. In an attempt to improve these constraints, a multi-parameter likelihood function is constructed that incorporates the nuisance parameters and the POI on an almost equal footing. In this high-dimensional parameter space, the likelihood is maximized on the m_T or p_T^ℓ distributions of the W boson data. In the ATLAS reanalysis of M_W [83], the number of nuisance parameters is initially in the hundreds.

This method appears sophisticated and increases the accuracy with which the nuisance and the interesting parameters together describe the m_T and p_T^ℓ distributions. However, the interpretation of the inferred M_W and its uncertainties is now opaque since it is mixed with hundreds of other parameters. The causal interpretation of the nuisance parameters may be lost if all parameters including M_W are reduced to mere smoothing knobs to fit a set of kinematic distributions. This raises the concern that M_W is getting tuned to smooth out internal inconsistencies, thereby losing its rigorous interpretation as a measured quantity. Similar concerns arise in the context of “over-fitting” in the parametric modeling of data [84, 85].

These issues worsen as the dimensionality of the nuisance parameter space increases; even if the initial choice of hundreds of parameters is pruned to 218, as in the ATLAS analysis, the post-fit likelihood function is still impossible to visualize and scrutinize. Mathematically, there is no guarantee that a 218-dimensional likelihood function is well-behaved in the entire domain bounded by the *a-priori* uncertainties on the nuisance parameters; i.e. that there is a stable global minimum without the existence of local minima, under-constrained “valleys” and saddle points which can lead to chaotic paths in the numerical minimization. Such issues may lead to a “random walk” of M_W of $\mathcal{O}(\sqrt{N}\delta)$ amounting to tens of MeV, where N is the (large) number of nuisance parameters floated simultaneously in the likelihood function and δ is a typical M_W deviation of a few MeV induced by each of them. Is one able to *a priori* defend the hypothesis-testing ability of a method which relies on a single POI that is susceptible to a random walk in a huge, 200+ dimensional parameter space?

The point is that, if the nuisance parameters are not correlated with the POI, there is no need to float them simultaneously with the POI. If they are correlated with the POI, then it is dangerous to float them simultaneously with the POI. In either case, the more robust procedure is to determine nuisance parameters from control samples of data, not the data used to determine the POI.

The purpose of high-dimensional machine-learning models is to provide a reproduction of training data, i.e. a method of mimicking data rather than a method of learning fundamental

principles governing the data. There is a rapidly growing forum in computer science related to interpretability and explainability of black box machine learning models. Explainable models allow human users to comprehend how the model is extracting information from the data and to debate if the model and its results can be trusted. Explainability is a requirement when a parameter that has a fundamental meaning is inferred from the data. CDF has maintained this philosophy of explainability for all its M_W measurements and will continue to do so in the future.

In the M_W context, it is important to understand the causal source of information in multi-parameter fitting, such as the reduction of the M_W uncertainty due to proton structure in the ATLAS analysis from *a-priori* 28 MeV to 8 MeV after the multi-parameter fit [83]. Which aspects of the m_T and p_T^ℓ distributions are constraining which degrees of freedom pertaining to the proton structure? Are these constrained degrees of freedom consistent with other world data describing the proton structure?

It would be interesting to understand the stability of multi-parameter fitting and to compare what one seems to learn from such fitting to what one expects to learn based on first-principles reasoning. The Fisher information is a measure of how much information about any model parameter is carried by the data. Evaluating the Fisher information for the nuisance parameters can help understand if multi-parameter fitting is resulting in legitimate or spurious constraints.

Using simulated data in which the ground truth is known by design, the likelihood-fitting approaches used by the Tevatron and LHC experiments could be compared. Among other insights, this study could help understand why re-fitting the same data published in 2018 [56, 57] by ATLAS with identical calibrations caused a 16 MeV shift [83] in the extracted M_W – the only change was that nuisance parameters were floated during M_W extraction. Similarly, M_W changes by 39 MeV in the LHCb analysis when an additional parameter ascribed to the p_T^W spectrum is floated simultaneously [58]. Could these shifts be a symptom of fitting instability in the black-box approach? The spectre of jumping between local minima in the loss function haunts the use of multi-parameter fitting.

3.6 Comparisons of M_W analyses at hadron colliders

The preceding sections discussed key aspects of M_W analyses and comparisons between how different experiments addressed them. Table 1 summarizes these comparisons, along with references to the respective sections.

4 Experience of M_W measurements

The prerequisite for higher precision measurements of M_W is the increase of the dataset size. It is also a learning experience because reducing the statistical error is only useful if the uncertainties due to nuisance parameters (i.e. systematic uncertainties) are also reduced, and this requires a deeper and more informed analysis. In other words, achieving precision is as much dependent on climbing a long learning curve as having more data.

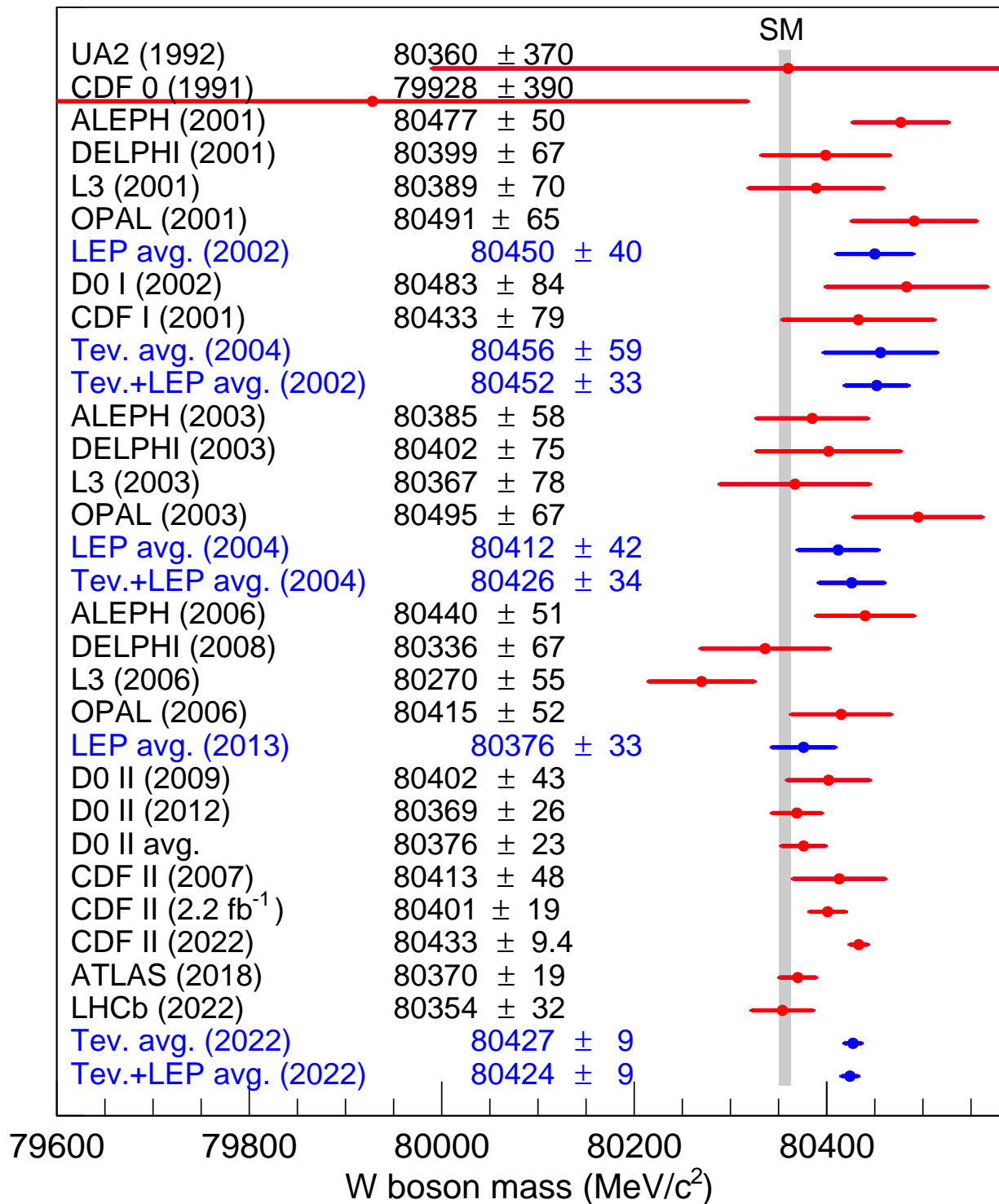


Figure 2: M_W measurements and the SM expectation. The latter includes the estimated uncertainty (4 MeV) due to higher-order effects in perturbation theory, and the uncertainty (4 MeV) induced by the experimental inputs to the calculation, such as the top quark mass. “Tev.” refers to the CDF and DØ experiments at the Fermilab Tevatron. Experimental measurements and their total uncertainties are shown as red points and averages of two or more experimental measurements are shown as blue points. ALEPH, DELPHI, and L3 measurements at CERN LEP are reanalyses of the full dataset (1995–2000), while OPAL’s 2001 and 2003 results used the first 60% of the full dataset. DØ measurements are published from independent data collected during successive Tevatron running periods. CDF II measurements are published using cumulative datasets so that all available CDF II data are analyzed for each publication. For the Tevatron experiments, “I” and “II” refer to the 1992–95 and 2000–2011 running periods respectively. The CDF II (2.2 fb⁻¹) value is from [15]. The measurements from the UA1 experiment [23] of $M_W = 82.7 \pm 1.0_{\text{stat}} \pm 2.7_{\text{syst}}$ (81.8^{+6.0}_{-5.3}(stat) ± 2.6_{syst}) GeV/c² in the electron (muon) channel would be plotted to the right of this figure.

Criterion	CDF	DØ	ATLAS	LHCb
sensitivity to proton structure (Sec. 3.1)	low	low	high	high
sensitivity to heavy quark effects (Sec. 3.1)	low	low	high	high
electron channel analyzed	yes	yes	yes	no
muon channel analyzed	yes	no	yes	yes
check of p_T^Z model with data (Sec. 3.1)	yes	yes	yes	yes
check of p_T^W/p_T^Z ratio with data (Sec. 3.1)	strong	no	weak	no
emphasis on tracker alignment (Sec. 3.2)	yes	no	no	no
momentum calibration using J/ψ and Υ (Sec. 3.2)	yes	no	no	partial
independent M_Z measurement & confirmation (Sec. 3.2)	yes	no	no	no
event selection bias corrections (Sec. 3.3)	small	large	large	large
recoil validation with m_T , p_T^ℓ & p_T^ν fits (Sec. 3.4)	strong	modest	weak	no
M_W -independent nuisance parameter constraints (Sec. 3.5)	yes	yes	no	no
dimensionality of M_W -inference likelihood (Sec. 3.5)	1	1	218	8
explainability of M_W inference procedure (Sec. 3.5)	high	high	low	low

Table 1: Comparisons of M_W analyses performed by various experiments at hadron colliders.

The progress on both fronts is notable in Fig. 2. Starting with the UA1 and UA2 experiments at the CERN $Spp\bar{S}$ collider, hadron colliders have reduced the uncertainties from all sources by two orders of magnitude. During these decades, better understanding of measurement procedures and nuisance parameters has occasionally shifted the value of a new measurement by more than the estimated uncertainty on the previous measurement. For example, the CDF measurement from the first quarter of the Tevatron Run 2 dataset appears to be shifted low by 33 MeV compared to their high-precision measurement from the full dataset [15]. As their analysis techniques improved substantially together with a quadrupling of the data, it would be useful for CDF to investigate if there is a causal explanation for the shift, which would contribute to scientific learning. In the same vein, the shift of 16 MeV in the ATLAS measurement due solely to an updated likelihood estimator, and the shift of 39 MeV in the LHCb measurement due to an additional floated parameter ascribed to the p_T^W spectrum, are worth understanding at a deeper level.

Measurements of M_W have also been performed at the LEP collider at CERN using two different methods. In the first method, M_W is inferred from the rise of the WW pair-production cross section when the electron-positron beam energies are scanned across the WW pair-mass threshold [32, 33, 34, 35]. These measurements were limited by the dataset size, but this threshold-scan technique is a robust and accurate method of measuring M_W . It could be repeated with extreme precision (≈ 0.5 MeV) at a future electron-positron collider designed to run at much higher luminosity [88]. The threshold-scan measurement of M_W is a prime motivator for such a future collider.

The second method of measuring M_W at LEP used the reconstructed 4-momenta of the final-state hadrons and charged leptons emanating from the decay of the pair-produced W

bosons. When both W bosons decay hadronically, strong interactions between the decay products from the two W bosons create a bias in the inferred M_W , which is corrected on the basis of hadronization models [32, 33, 34, 35]. Methods of attributing the measured particles' momenta to the respective W bosons evolved, as did the hadronization models [28, 29, 30, 31]. Between 2003 and 2006-8, all four LEP experiments updated their measurements by ≈ 75 MeV or $\gtrsim 1\sigma$ each, as seen in Fig. 2 [86, 87, 36]. In preparation for a new electron-positron collider, revisiting the origin of these rather substantial shifts would be educational.

The lesson learnt is that understanding and control of nuisance parameters is crucial in all M_W analyses, both at lepton and hadron colliders.

4.1 Prospects

The experiments running at the LHC are technologically advanced and can be calibrated with careful analysis of *in-situ* control samples of data. They have already collected two orders of magnitude larger data samples than the Tevatron, and another order of magnitude increase is expected from future running. However, these samples will suffer from a large rate of pile-up events because they have been or will be collected with a high beam luminosity which enables the large signal sample rate. Ironically, the requirements of the M_W measurement from the perspective of precision and robustness are better served by a lower beam energy to simplify the W boson production dynamics and a lower beam luminosity to reduce pile-up. While the technical and scientific cost to the rest of the LHC physics program may outweigh the benefit of a lower beam energy, a short-term reduction in the beam luminosity is an attractive option. Data collected at low luminosity will reduce the number of additional proton-proton collisions that complicate the inference of the neutrino momentum. Among other benefits, low-luminosity data will provide the built-in consistency check of M_W extracted from the m_T , p_T^ℓ and p_T^ν distributions, which is only possible when the p_T^ν resolution is not degraded by pile-up.

In the longer term, an electron-positron collider that serves as a Higgs and electroweak factory will be the ultimate precision machine for the measurement of W , Z and Higgs boson properties [89, 90, 91, 92]. The beam-energy scan at the WW pair-production threshold is the most robust method of confirming the difference between the measured M_W and its SM-calculated value [88]. This difference is most striking in the recent CDF measurement, but Fig. 2 shows the historical trend for this difference to be positive.

The M_W measurement at this future collider complements an extensive program of precision measurements of Z bosons which can improve upon the precision achieved at LEP by a factor of 20–100 [92]. Similarly, certain properties of the Higgs boson can be measured with precision ranging from 1% to 0.2%, exceeding the capability of the LHC in these respects [92]. As with M_W , the motivation for making extremely precise measurements of such observables is that they can be calculated with commensurately high precision in the SM. A pattern of deviations between measured and calculated values may emerge that guides us to develop a deeper theory that subsumes and supersedes the SM.

4.2 Weak mixing angle

In Sec. 2 we discussed how the SM predicts the value of M_W when other key parameters are fixed by measurements. We mentioned the weak mixing angle that describes the superposition of two generators of the $SU(2)_{\text{weak}}$ and $U(1)_{\text{hypercharge}}$ gauge groups respectively. The SM also predicts the weak mixing angle when the above-mentioned parameters are fixed [93]; thus, a precise measurement of the weak mixing angle provides a stringent test of the SM, along the same lines as and independent of M_W .

The two most precise measurements of the weak mixing angle have been performed in the 1990s by the LEP experiments and by the SLD experiment at the SLAC SLC accelerator respectively [94]. The measurements were based on different properties of Z bosons; the SLD observable depends on leptonic couplings only, while the LEP observable involves b -quark couplings. The measurements differ by 3.2σ . The SLD measurement relies on beam polarization and the LEP measurement relies on identification of b -quarks produced from the Z boson decay.

This discrepancy has not been resolved; nevertheless the two measurements have been averaged. Additional measurements have been made in atomic parity violation, electron and neutrino scattering, and at the Tevatron and LHC (see [16] for a review). Analysis of the available LHC data may yield a precision similar to that of the SLD measurement. New experiments [95, 96, 97] including those at a future electron-positron collider [89, 90, 91, 92] plan to improve upon the precision of this parameter.

In the meantime, the status of this discrepancy in the weak mixing angle is similar to the $\sim 3\sigma$ difference between the CDF and ATLAS measurements of M_W . Per precedence, the scientific approach is to combine the M_W measurements using established statistical methods while continuing investigations. This approach has been applied when even larger differences, such as the 5.5σ between measurements of the fine structure constant α using Cesium and Rubidium atoms, have been found [16]. An alternate, biased approach has been presented in [98]. Unless scientific concerns on any published result are documented, it is not scientific practice to isolate any measurement as an outlier and remove it from a world average. The Particle Data Group has maintained a time-tested procedure for combining measurements that are not in perfect agreement - the PDG review is replete with examples [16].

It is interesting to note that the SLD measurement of the weak mixing angle and the CDF measurement of M_W each point towards the same new physics, qualitatively and quantitatively. This concurrence (Fig. 3) has been pointed out in [99], where it is shown that both measurements favor a similar violation of the WZ custodial symmetry that we discussed in Sec. 2 as an approximate feature of the SM.

4.3 Muon magnetic moment

Analogous to M_W and $\sin^2 \theta_{\text{eff}}$, the magnetic moments of the electrons and the muon are precisely measurable and their values are predicted by the SM. The magnetic moment is proportional to the intrinsic spin, the charge/mass ratio and the g -factor, where $g = 2$ in Dirac's theory of the electron. In quantum field theory this prediction is modified by

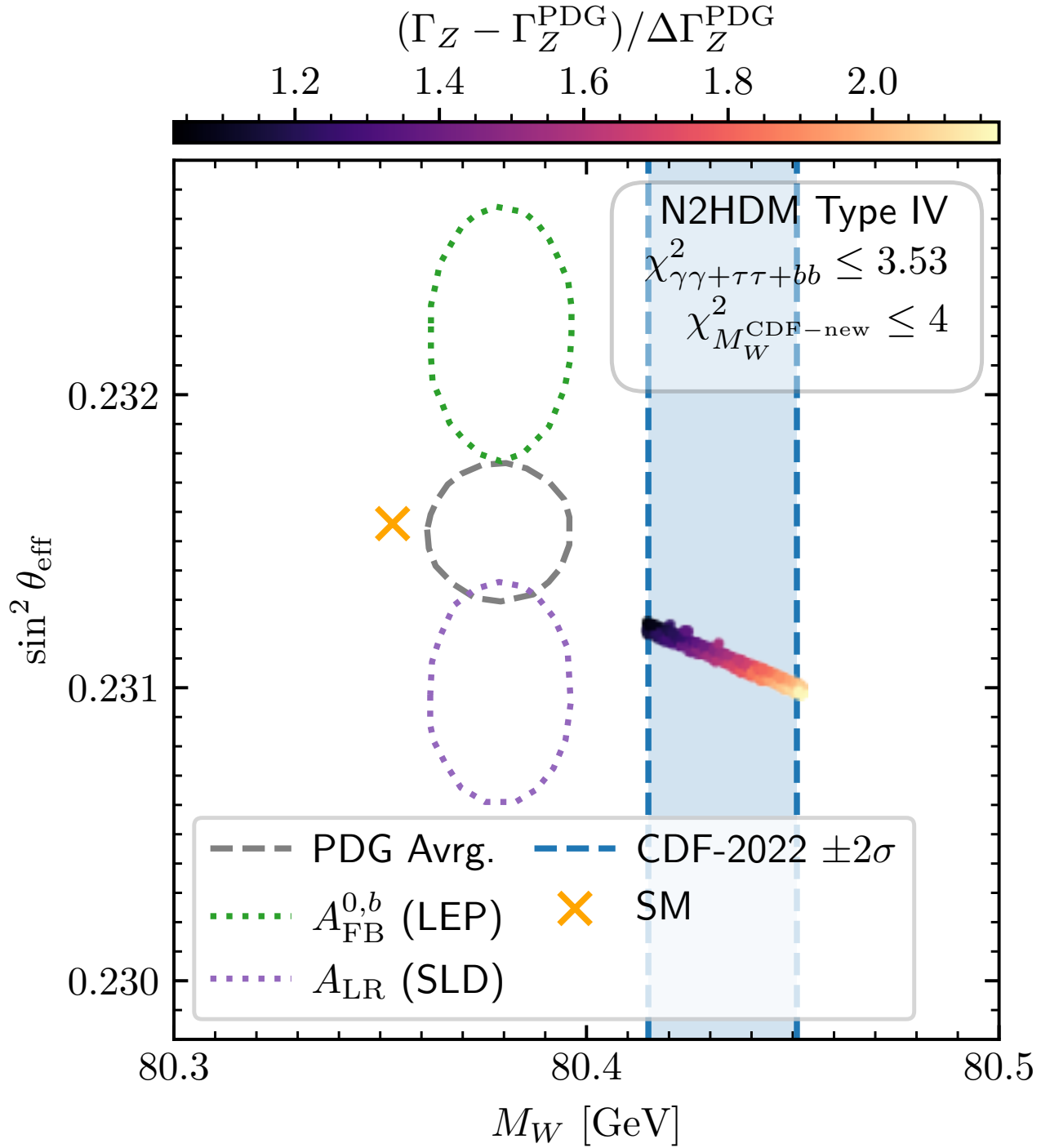


Figure 3: Illustration (reproduced with permission from Fig. 2 of Ref. [99]) of the two most precise measurements of the weak mixing angle θ_{eff} (shown conventionally as $\sin^2 \theta_{\text{eff}}$ on the vertical axis) from the LEP experiments and the SLD experiment respectively [94], and their average [16]. The CDF measurement of the W boson mass is shown on the horizontal axis. The SM expectation is shown as the orange cross. The SLD measurement of $\sin^2 \theta_{\text{eff}}$ and the CDF measurement of M_W concur on a set of new-physics scenarios shown as the line of colored points. While a supersymmetric framework with additional Higgs bosons is used in [99], the common feature between these and other models is the violation of WZ custodial symmetry mentioned in Sec. 2.

quantum fluctuations which are calculable as a perturbation series with the electromagnetic fine structure constant α as the expansion parameter. A measurement of $(g-2)$ is a stringent test of the SM and has been pursued for both electrons and muons for many decades, along with increasing accuracy of its calculations.

In recent years, a difference between the measured and calculated values of muon $(g-2)$ has been reported [100, 101, 102, 103]. The most recent measurement from Fermilab [100] improves the precision of the experimental world average by a factor of two. Simultaneously, the SM calculation of this quantity is being revisited [104] due to improved inputs from QCD calculations on the lattice [105, 106] and from a new measurement of the $e^+e^- \rightarrow \pi^+\pi^-$ cross section near threshold [107]. This information changes the hadronic vacuum polarization and the resulting update to α would bring the SM value of the muon $(g-2)$ closer to the measured value.

The effect of low-energy hadronic quantum fluctuations on α propagate to M_W and to the muon $(g-2)$ in opposite directions [108]. In other words, if the discrepancy between the measured and calculated values were to reduce for the muon $(g-2)$ due to an adjustment of α , the discrepancy must increase for *all* M_W measurements, and vice versa. There is no way to reconcile both discrepancies simultaneously by adjusting this hadronic quantum correction on α .

The interesting conclusion is that the combination of these two measurements makes a striking case for new physics. Whether the new physics manifests in the muon’s magnetic moment, or the W boson mass, or both, these two measurements are hinting at a future beyond the Higgs boson.

5 Summary

Developed over a century, the SM is one of the crowning achievements of science. It is built on a remarkable set of axioms of local quantum field theory, special relativity and group theory, and has been both strongly guided by and predictive of a vast set of experimental observations. The SM’s theoretical structure and past consistency with experimental data together led to the prediction of the Higgs boson, which was spectacularly confirmed by its observation at the LHC in 2012.

Nevertheless, the SM is not expected to be the most fundamental theory of matter and forces. The Higgs sector of the SM is not as axiomatic as the rest of the theory; the Higgs field’s fermionic- and self-interactions are parametrized phenomenologically without a fully dynamical construction. Second, the parameter describing the Higgs boson mass receives large quantum corrections that are very sensitive to unknown physics at arbitrarily high energy scales. The small observed value of the Higgs boson mass raises the concern of “naturalness” of the Higgs sector, because it requires an extremely tuned set of conditions at higher energies. Such “fine-tuning” is prevented in other sectors of the SM by its symmetry structure [109], and can be alleviated for the Higgs mass parameter as well by extending the field content and symmetries of the theory. The fine-tuning associated with the Higgs mass

increases quadratically with the energy scale of new physics, which creates an expectation that the new physics is around the corner.

Another set of deficiencies in the SM relate to crucial facts of cosmological significance - the observed excess of matter over antimatter in the universe, dark matter, dark energy and cosmic inflation, all of which are beyond the scope of the SM. Finally, the force of gravity cannot be accommodated into the SM's quantum field-theoretic framework.

For such reasons, physics beyond the SM is expected to show up. *A-priori* there is no definitive prediction for the energy scale at which new physics may be revealed. Nevertheless, these considerations justify current and future particle physics experiments that are designed to observe phenomena not explainable by the SM.

We discussed the theoretical reasoning for the W boson mass to be a sensitive probe of certain aspects of new physics, which explains why this measurement has been pursued with increasing precision (progressing by two orders of magnitude) over the last three decades. Finally we have an M_W measurement that shows a significant tension; it is the largest deviation observed from a prediction of the SM. The most exciting possibility is that the new physics that this deviation points towards will reveal itself as new particles in the near future.

Acknowledgements

We thank Kaustubh Agashe, Sunil Gupta and Ronen Plesser for helpful discussions.

References

- [1] C. S. Wu, E. Ambler, R. W. Hayward, D. D. Hoppes, R. P. Hudson. *Phys. Rev.* **105** (4), 1413-1415 (1957).
- [2] P. W. Anderson, *Phys. Rev.* **130**, 439 (1963).
- [3] F. Englert and R. Brout, *Phys. Rev. Lett.* **13**, 321 (1964).
- [4] P. W. Higgs, *Phys. Rev. Lett.* **13**, 508-509 (1964).
- [5] P. W. Higgs, *Phys. Lett.* **12**, 132-133 (1964).
- [6] G. S. Guralnik, C. R. Hagen, and T. W. B. Kibble, *Phys. Rev. Lett.* **13**, 585 (1964).
- [7] G. Aad *et al.* (ATLAS Collaboration), *Phys. Lett. B* **716**, 1 (2012).
- [8] S. Chatrchyan *et al.* (CMS Collaboration), *Phys. Lett. B* **716**, 30 (2012).
- [9] S. Glashow, *Nucl. Phys.* **22**, 579 (1961).
- [10] A. Salam and J. C. Ward, *Phys. Lett.* **13**, 168 (1964).
- [11] S. Weinberg, *Phys. Rev. Lett.* **19**, 1264 (1967).

- [12] G. P. Salam, LT. Wang, & G. Zanderighi, *Nature* **607**, 41-47 (2022).
- [13] The ATLAS Collaboration. *Nature* **607**, 52-59 (2022).
- [14] The CMS Collaboration. *Nature* **607**, 60-68 (2022).
- [15] T. Aaltonen *et al.* (CDF Collaboration), *Science* **376**, 170-176 (2022).
- [16] R. L. Workman *et al.* (Particle Data Group), *Prog. Theor. Exp. Phys.* **2022**, 083C01 (2022).
- [17] M. Awramik, M. Czakon, A. Freitas, and G. Weiglein, *Phys. Rev. D* **69**, 053006 (2004).
- [18] J. Erler and M. Schott, *Progress in Particle and Nuclear Physics* **106**, 68 (2019).
- [19] G. Arnison *et al.* (UA1 Collaboration), *Phys. Lett. B* **122**, 103 (1983).
- [20] M. Banner *et al.* (UA2 Collaboration), *Phys. Lett. B* **122**, 476 (1983).
- [21] G. Arnison *et al.* (UA1 Collaboration), *Phys. Lett. B* **126**, 398 (1983).
- [22] P. Bagnaia *et al.* (UA2 Collaboration), *Phys. Lett. B* **129**, 130 (1983).
- [23] C. Albajar *et al.* (UA1 Collaboration), *Z. Phys. C* **44**, 15 (1989).
- [24] R. Ansari *et al.* (UA2 Collaboration), *Phys. Lett. B* **186**, 440 (1987).
- [25] J. Alitti *et al.* (UA2 Collaboration), *Phys. Lett. B* **276**, 354 (1992).
- [26] F. Abe *et al.* (CDF Collaboration), *Phys. Rev. Lett.* **65**, 2243 (1990).
- [27] F. Abe *et al.* (CDF Collaboration), *Phys. Rev. D* **43**, 2070 (1991).
- [28] R. Barate *et al.* (ALEPH Collaboration), *Eur. Phys. J. C* **17**, 241 (2000).
- [29] P. Abreu *et al.* (DELPHI Collaboration), *Phys. Lett. B* **511**, 159 (2001).
- [30] M. Acciarri *et al.* (L3 Collaboration), *Phys. Lett. B* **454**, 386 (1999).
- [31] G. Abbiendi *et al.* (OPAL Collaboration), *Phys. Lett. B* **507**, 29 (2001).
- [32] S. Schael *et al.* (ALEPH Collaboration), *Eur. Phys. Jour. C* **47**, 309 (2006).
- [33] J. Abdallah *et al.* (DELPHI Collaboration), *Eur. Phys. Jour. C* **55**, 1 (2008).
- [34] P. Achard *et al.* (L3 Collaboration), *Eur. Phys. Jour. C* **45**, 569 (2006).
- [35] G. Abbiendi *et al.* (OPAL Collaboration), *Eur. Phys. Jour. C* **45**, 307 (2006).

- [36] The ALEPH Collaboration, The DELPHI Collaboration, The L3 Collaboration, The OPAL Collaboration, The LEP Electroweak Working Group, *Phys. Rept.* **532** (4), 118 (2013).
- [37] F. Abe *et al.* (CDF Collaboration), *Phys. Rev. Lett.* **75**, 11 (1995).
- [38] F. Abe *et al.* (CDF Collaboration), *Phys. Rev. D* **52**, 4784 (1995).
- [39] T. Affolder *et al.* (CDF Collaboration), *Phys. Rev. D* **64**, 052001 (2001).
- [40] S. Abachi *et al.* (D0 Collaboration), *Phys. Rev. Lett.* **77**, 3309 (1996).
- [41] B. Abbott *et al.* (D0 Collaboration), *Phys. Rev. D* **58**, 012002 (1998).
- [42] B. Abbott *et al.* (D0 Collaboration), *Phys. Rev. Lett.* **80**, 3008 (1998).
- [43] B. Abbott *et al.* (D0 Collaboration), *Phys. Rev. D* **58**, 092003 (1998).
- [44] B. Abbott *et al.* (D0 Collaboration), *Phys. Rev. Lett.* **84**, 222 (2000).
- [45] B. Abbott *et al.* (D0 Collaboration), *Phys. Rev. D* **62**, 092006 (2000).
- [46] V. M. Abazov *et al.* (D0 Collaboration), *Phys. Rev. D* **66**, 012001 (2002).
- [47] V. M. Abazov *et al.* (CDF and D0 Collaborations), *Phys. Rev. D* **70**, 092008 (2004).
- [48] T. Aaltonen *et al.* (CDF Collaboration), *Phys. Rev. Lett.* **99**, 151801 (2007).
- [49] T. Aaltonen *et al.* (CDF Collaboration), *Phys. Rev. D* **77**, 112001 (2008).
- [50] T. Aaltonen *et al.* (CDF Collaboration), *Phys. Rev. Lett.* **108**, 151803 (2012).
- [51] T. Aaltonen *et al.* (CDF Collaboration), *Phys. Rev. D* **89**, 072003 (2014).
- [52] V. M. Abazov *et al.* (D0 Collaboration), *Phys. Rev. Lett.* **103**, 141801 (2009).
- [53] V. M. Abazov *et al.* (D0 Collaboration), *Phys. Rev. Lett.* **108**, 151804 (2012).
- [54] V. M. Abazov *et al.* (D0 Collaboration), *Phys. Rev. D* **89**, 012005 (2014).
- [55] T. Aaltonen *et al.* (CDF and D0 Collaborations), *Phys. Rev. D* **88**, 052018 (2013).
- [56] M. Aaboud *et al.* (ATLAS Collaboration), *Eur. Phys. J. C* **78**, 110 (2018).
- [57] M. Aaboud *et al.* (ATLAS Collaboration), erratum *Eur. Phys. J. C* **78**, 898 (2018).
- [58] R. Aaij *et al.* (LHCb Collaboration), *J. High Energ. Phys.* **2022**, 36 (2022).
- [59] W. J. Marciano and A. Sirlin, *Phys. Rev. D* **22**, 2695 (1980); erratum *Phys. Rev. D* **31**, 213 (1985).

- [60] D. A. Ross, M. J. G. Veltman, *Nucl. Phys. B* **95**, 135 (1975).
- [61] G. 't Hooft and M. Veltman. *Nucl. Phys. B* **44**, 189-213 (1972).
- [62] M. J. G. Veltman, *Nucl. Phys. B* **123** 1, 89-99 (1977).
- [63] J. Erler and P. Langacker, *Phys. Rev. D* **52**, 441 (1995).
- [64] F. Abe *et al.* (CDF Collaboration), *Phys. Rev. Lett.* **74**, 2626 (1995).
- [65] S. Abachi *et al.* (DØ Collaboration), *Phys. Rev. Lett.* **74**, 2632 (1995).
- [66] M. J. G. Veltman, *Acta Phys. Polon. B* **25** 1627-1636 (1994).
- [67] D. J. Gross & F. Wilczek, *Phys. Rev. Lett.* **30**, 1343-1346 (1973).
- [68] H. D. Politzer, *Phys. Rev. Lett.* **30**, 1346-1349 (1973).
- [69] C. Balázs and C.-P. Yuan, *Phys. Rev. D* **56**, 5558 (1997).
- [70] G. A. Ladinsky and C.-P. Yuan, *Phys. Rev. D* **50**, R4239 (1994).
- [71] F. Landry, R. Brock, P. M. Nadolsky, and C.-P. Yuan, *Phys. Rev. D* **67**, 073016 (2003).
- [72] The CDF 2022 measurement uses the latest version of the RESBOS program, colloquially referred to as RESBOS2, with next-to-next-to-leading logarithm resummation and next-to-leading order accuracy in QCD in the vector boson production and decay.
- [73] G. Bozzi, S. Catani, G. Ferrera, D. de Florian, M. Grazzini, *Nucl. Phys. B* **815**, 174-197 (2009).
- [74] G. Bozzi, S. Catani, G. Ferrera, D. de Florian, M. Grazzini, *Phys. Lett. B* **696**, 207-213 (2011).
- [75] We thank Davison Soper, John Collins and Tao Han for this suggestion.
- [76] Private communication from the DØ Collaboration.
- [77] T. Affolder *et al.*, *Nucl. Instrum. Methods Phys. Res. A* **526**, 249 (2004).
- [78] A. V. Kotwal, H. K. Gerberich, and C. Hays, *Nucl. Instrum. Methods Phys. Res. A* **506**, 110 (2003).
- [79] A. V. Kotwal and C. Hays, *Nucl. Instrum. Methods Phys. Res. A* **762**, 85 (2014).
- [80] A. V. Kotwal and C. Hays, *Nucl. Instrum. Methods Phys. Res. A* **729**, 25 (2013).
- [81] R. Brun, F. Bruyant, F. Carminati, S. Giani, M. Maire, A. McPherson, G. Patrick and L. Urban, CERN Program Library Long Writeup, W5013 (1993), version 3.15, <https://cds.cern.ch/record/1082634>

- [82] S. Agostinelli *et al.*, *Nucl. Instrum. Methods Phys. Res. A* **506**, 250 (2003).
- [83] ATLAS Collaboration, ATLAS-CONF-2023-004 (2023).
- [84] K. P. Burnham and D. R. Anderson, “Model Selection and Multimodel Inference” (2nd ed.), Springer (2002).
- [85] F. Dyson, *Nature* **427**, 297 (2004). The author quotes Enrico Fermi’s recollection of a statement by John von Neumann that four complex parameters can fit an elephant and five complex parameters can describe an elephant wiggling its trunk.
- [86] The LEP Collaborations ALEPH, DELPHI, L3, OPAL, the LEP Electroweak Working Group, the SLD Electroweak and Heavy Flavour Groups, arXiv:hep-ex/0112021v2 (2002).
- [87] The LEP Collaborations ALEPH, DELPHI, L3, OPAL, the LEP Electroweak Working Group, the SLD Electroweak and Heavy Flavour Groups, arXiv:hep-ex/0312023v2 (2004).
- [88] P. Azzurri, *Eur. Phys. J. Plus* **136**, 1203 (2021).
- [89] ILC International Development Team Collaboration, A. Aryshev *et al.*, arXiv:2203.07622 [physics.acc-ph].
- [90] CEPC Physics Study Group, H. Cheng *et al.*, arXiv:2205.08553 [hep-ph].
- [91] CLIC Collaboration, J. de Blas *et al.*, arXiv:1812.02093 [hep-ph].
- [92] A. Blondel & P. Janot, *Eur. Phys. J. Plus* **137**, 92 (2022).
- [93] A. Sirlin, *Phys. Rev. D* **22**, 971 (1980).
- [94] The ALEPH Collaboration, The DELPHI Collaboration, The L3 Collaboration, The OPAL Collaboration, The SLD Collaboration, The LEP Electroweak Working Group, The SLD Electroweak and Heavy Flavour Groups, *Phys. Rept.* **427**, 257 (2006).
- [95] J. Benesch *et al.*, (MOLLER Collaboration), arXiv:1411.4088 [nucl-ex].
- [96] J. Arrington *et al.* (SoLID), arXiv:2209.13357 [nucl-ex].
- [97] D. Becker *et al.* (P2), *Eur. Phys. J. A* **54**, 208 (2018).
- [98] S. Amoroso *et al.*, arXiv:2308.09417 (2023).
- [99] T. Biekötter, S. Heinemeyer & G. Weiglein, *Eur. Phys. J. C* **83**, no. 5, 450 (2023).
- [100] D. P. Aguillard *et al.* (Muon $g-2$ Collaboration), arXiv:2308.06230 (2023), submitted for publication in *Phys. Rev. Lett.*

- [101] B. Abi *et al.* (Muon $g - 2$ Collaboration), *Phys. Rev. Lett.* **126**, 141801 (2021).
- [102] T. Albahri *et al.* (Muon $g - 2$ Collaboration), *Phys. Rev. D* **103**, 072002 (2021).
- [103] G. W. Bennett *et al.* (Muon $g - 2$ Collaboration), *Phys. Rev. D* **73**, 072003 (2006).
- [104] D. Castelvecchi, *Nature* **620**, 473-474 (2023).
- [105] S. Borsanyi, *et al.* (BMW Collaboration), *Nature* **593**, 51-55 (2021).
- [106] C. Lehner, *Nat Rev Phys* **4**, 14-15 (2022).
- [107] F. V. Ignatov *et al.* (CMD-3 Collaboration), arXiv:2302.08834 (2023).
- [108] P. Athron, A. Fowlie, CT. Lu *et al.*, *Nat Commun* **14**, 659 (2023).
- [109] Gerard 't Hooft. NATO *Sci. Ser. B* **59**, 135 (1980).